energies

Article

Transient Synchronous Stability Analysis of Grid-Forming Photovoltaic Grid-Connected Inverters during Asymmetrical Grid Faults

Wenwen He [1], Jun Yao [1,*], Hao Xu [1], Qinmin Zhong [1], Ruilin Xu [2], Yuming Liu [2] and Xiaoju Li [2]

[1] State Key Laboratory of Power Transmission Equipment Technology, School of Electrical Engineering, Chongqing University, Chongqing 400044, China
[2] State Grid Chongqing Electric Power Research Institute, Chongqing 400044, China
* Correspondence: jyao@cqu.edu.cn

Abstract: Compared with the traditional grid-following photovoltaic grid-connected converter (GFL-PGC), the grid-forming photovoltaic grid-connected converter (GFM-PGC) can provide voltage and frequency support for power systems, which can effectively enhance the stability of power electronic power systems. Consequently, GFM-PGCs have attracted great attention in recent years. When an asymmetrical short-circuit fault occurs in the power grid, GFM-PGC systems may experience transient instability, which has been less studied so far. In this paper, a GFM-PGC system is investigated under asymmetrical short-circuit fault conditions. A novel *Q-V* droop control structure is proposed by improving the traditional droop control. The proposed control structure enables the system to accurately control the positive- and negative-sequence reactive current without switching the control strategy during the low-voltage ride-through (LVRT) period so that it can meet the requirements of the renewable energy grid code. In addition, a dual-loop control structure model of positive- and negative-sequence voltage and current is established for the GFM-PGC system under asymmetrical short-circuit fault conditions. Based on the symmetrical component method, the composite sequence network of the system is obtained under asymmetrical short-circuit fault conditions, and positive- and negative-sequence power-angle characteristic curves are analyzed. The influence law of system parameters on the transient synchronous stability of positive- and negative-sequence systems is quantitatively analyzed through the equal area criterion. Finally, the correctness of the theoretical analysis is verified by simulation and hardware-in-the-loop experiments.

Keywords: grid-forming photovoltaic grid-connected converter; transient synchronous stability; asymmetric grid faults; grid code

Citation: He, W.; Yao, J.; Xu, H.; Zhong, Q.; Xu, R.; Liu, Y.; Li, X. Transient Synchronous Stability Analysis of Grid-Forming Photovoltaic Grid-Connected Inverters during Asymmetrical Grid Faults. *Energies* **2024**, *17*, 1399. https://doi.org/10.3390/en17061399

Academic Editor: Alon Kuperman

Received: 18 February 2024
Revised: 11 March 2024
Accepted: 12 March 2024
Published: 14 March 2024

1. Introduction

Nowadays, traditional energy sources are being replaced by renewable energy sources due to issues related to climate conditions and environmental changes [1,2]. Renewable energy sources such as photovoltaics have been connected to the power system through photovoltaic grid-connected converters (PGCs) in large quantities. The penetration rate of power electronic devices in power systems has been increasing, and the dominance of synchronous generators (SGs) has gradually decreased [3–5]. Due to the transition from rotating machinery-based SGs to inverter-based resources, the mechanical inertia of power systems has been reduced, which is a concern of grid operators [6]. The reduction in stored energy in a rotating rotor leads to larger frequency swings during load disturbances, which can trip the load or inverter-based units [6,7]. Therefore, the stability of power systems will be reduced during grid faults.

Currently, most commercial PGCs operate as grid-following (GFL) sources [7,8]. The traditional GFL-PGC is externally regarded as a controlled current source with high parallel impedance, and GFL-PGCs sample the voltage of the point of common coupling (PCC) during normal operations. The synchronization between GFL-PGCs and the power grid is realized through a phase-locked loop (PLL) [9,10]. However, it is difficult to effectively support the power grid using the control method based on GFL during grid frequency and voltage change [11]. As an alternative solution, GFM-PGC control has been gaining the attention of both academia and industry in recent years [12]. GFM control simulates the characteristics of synchronous generators, which can automatically generate voltage amplitude and phase by adjusting the output active power and reactive power [11]. PGCs can realize self-synchronous operation through the GFM control structure, which is conducive to improving the damping and inertia of power systems [13]. Hence, it is necessary to investigate the GFM-PGC system to enhance the stability of power systems with a high share of renewable energy.

The GFM-PGC externally presents as a controlled voltage source with low series impedance, and GFM-PGCs are connected to power grids through power self-synchronization control loops [14–17]. Under weak grid conditions, a GFM-PGC system has a larger stability margin. The GFM-PGC can operate both in islanded and grid-connected modes, which means that the GFM-PGC has a wider range of application scenarios. Although the control structures of the GFM-PGC are different, they all have the ability to establish AC-side output voltages without relying on grid voltage [18–20]. As a consequence, GFM-PGC systems can provide inertial and damping support for power electronic power systems, which is the reason GFM-PGC systems have been receiving widespread attention [21,22].

Currently, most of the studies on the stability of GFM-PGC systems are based on the steady-state operating conditions of the power grid [23,24]. When a large disturbance fault occurs in the grid, a GFM-PGC system will experience transient instability, which is similar to SG [25,26]. Under severe fault conditions, GFM-PGC systems can even avoid overvoltage and overcurrent by disconnecting from the grid or degrading to GFL-PGCs. Reference [27] proposed a current limitation strategy for GFM-PGC systems based on mode smooth switching, which turns a GFM-PGC into a GFL-PGC to limit the fault current during a fault period. However, the system is not able to provide frequency and voltage support for the grid. In order to realize the full process of grid-forming control, GFM-PGCs should be equipped with strong fault adaptability to provide transient voltage and frequency support for the power grid.

Some investigations have been carried out on the transient synchronous stabilization of GFM-PGCs during symmetrical faults in power systems. Reference [28] analyzed the effect of the damping coefficient and the droop control coefficient of a virtual synchronous generator (VSG) on the transient stability of a power system through Lyapunov's direct method, which pointed out that the Q-V droop link reduces the power-angle stabilization margin of VSGs. Reference [29] analyzed the transient stability of a VSG system under large disturbances using the equal area criterion, and an adaptive power-angle control method was proposed to improve the transient stability of VSG systems. Phase portraits were used to investigate the transient synchronous stabilization process of a GFM-PGC system [30], the influence of control parameters on the system's stability was analyzed, and a reference for the parameter design of the GFM-PGC system was provided. Considering the current limitation of transmission line faults, reference [31] proposed a two-stage synchronous control scheme to improve the transient stability of GFM-PGC systems. Reference [32] investigated the effect of a Q-V droop loop on the transient stability of a system using the equal area criterion, and an improved Q-V control structure was proposed to improve the transient stability of the system during grid faults. The above studies mainly investigated the effects of P-f and Q-V droop loops of GFM-PGC systems on the transient stability of the systems through phase portraits, the equal area criterion and the Lyapunov function method. Some improved control strategies have been proposed. Nevertheless, the probability of asymmetrical short-circuit faults is greater in real power grids, and the coupling between positive- and negative-sequence components will lead to a more complicated transient synchronous instability mechanism of GFM-PGC systems.

In order to fill the current research gaps, this paper investigates the transient synchronous stability of the GFM-PGC system during asymmetrical grid faults. The main contributions of this article are summarized below.

- Based on the symmetrical components method, a sequence-domain model of the GFM-PGC system is established, and general expressions of the positive- and negative-sequence active powers are formulated. On this basis, transient synchronous stability criteria of the positive- and negative-sequence systems are further proposed to evaluate the stability margin of the system.
- According to the mathematical model of the GFM-PGC system under asymmetrical short-circuit faults, a novel *Q-V* droop control strategy is proposed to improve the dynamic reactive power support capability. This strategy can inject positive- and negative-sequence reactive currents which meet the requirements of the renewable energy grid code [32,33].

This article is structured as follows. Section 2 introduces the modeling of GFM-PGC systems under asymmetrical grid faults. Section 3 analyzes the positive- and negative-sequence transient synchronous stability of GFM-PGC systems during asymmetrical short-circuit faults. Section 4 presents the simulation results. Section 5 is devoted to hardware-in-the-loop experiments. Section 6 concludes the article.

2. GFM-PGC System Modelling during Asymmetric Grid Faults

The main circuit and control structure of the GFM-PGC system are shown during an asymmetrical short-circuit fault period in Figure 1.

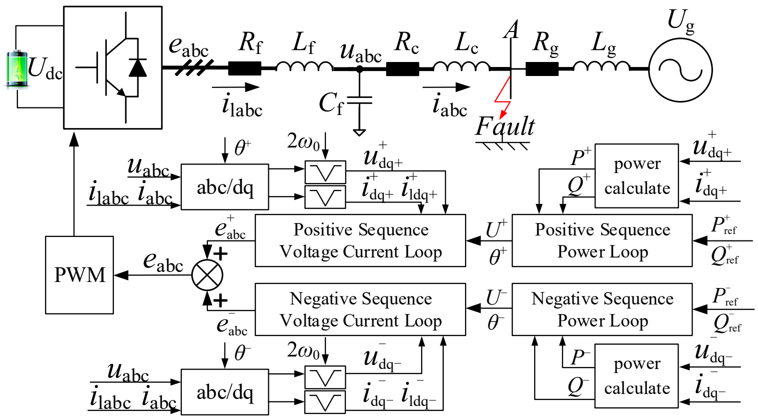

Figure 1. Main circuit and control structure of the GFM-PGC system.

In the above diagram, e_{abc} and i_{labc} are the voltage and current at the GFM-PGC port, respectively. u_{abc} represents the voltage at the LC filter, and i_{abc} is the output current. U_g is the AC bus voltage. L_f and C_f are the inductance and capacitance of the LC filter. R_f is the equivalent resistance of the LC filter. R_g, R_c, L_g and L_c are the equivalent resistances and inductances of the transmission line. P_{ref}^{+}, Q_{ref}^{+}, P_{ref}^{-} and Q_{ref}^{-} are the positive- and negative-sequence power reference values. P^{+}, Q^{+}, P^{-} and Q^{-} are the actual values of the inverter output active and reactive power. The asymmetric short circuit fault occurs at point A.

With the increasing proportion of PGCs in the power system, the stable operation capability of the power system may be reduced due to the fluctuation and intermittency of PGC systems. In order to solve the existing problems, equipping the energy storage system is an effective method to smooth the fluctuation in renewable energy and improve the adjustability of the renewable energy power supply. On this basis, the DC side of the PGC system can be equivalent to a stable DC voltage source. Therefore, this paper mainly analyzes the transient synchronous stability of the grid side of the PGC system.

2.1. Sequence-Domain Circuit of the GFM-PGC System during Asymmetrical Faults in the Power Grid

The GFM-PGC system generates the PCC voltage amplitude and phase through a power control loop. The system regulates the PCC voltage through an internal voltage and current control loop, which tracks the PCC voltage reference value and achieves overcurrent protection [34]. Generally, the bandwidth of the inner voltage and the current loop is much higher than that of the outer power control loop [34]. Thus, the voltage and current inner control loop can be regarded as a gain of the PCC voltage. The GFM-PGC is equivalent to a controlled voltage source.

The positive-, negative- and zero-sequence Thevenin equivalent networks of the GFM-PGC system are shown during an asymmetrical short-circuit fault in Figure 2. As can be seen, the converter is modeled to inject voltage in both the positive- and negative-sequences, and the external grid is assumed to only provide positive-sequence voltages [35]. Considering the complete transposition of the transmission lines, the positive-sequence and negative-sequence impedances are equal: $Z_L^+ = Z_L^- = Z_L^0/3 = |Z_L|\angle\varphi_L$.

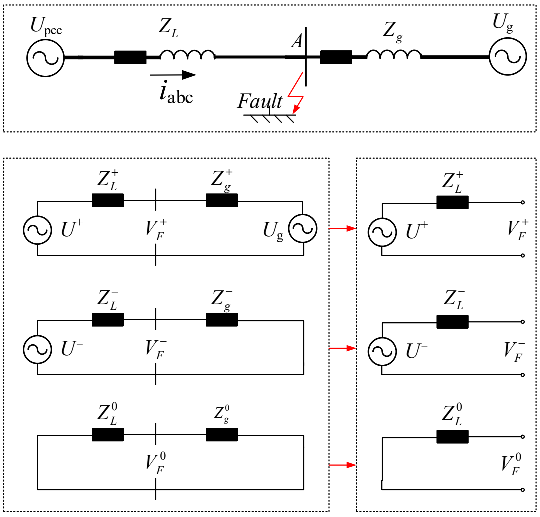

Figure 2. The Thevenin equivalents circuit of the GFM-PGC system during an asymmetrical short-circuit fault.

The system circuit diagram under a single line-to-ground (SLG) fault is shown in Figure 3.

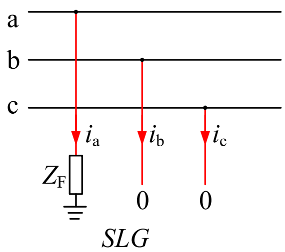

Figure 3. The system circuit diagram under an SLG fault.

Considering the SLG fault in Figure 3, the following boundary conditions exist: $i_b = i_c = 0$ and $V_{Fa} = Z_F i_a$. Based on the symmetrical components theory, the sequence components of the fault currents become:

$$\begin{bmatrix} I_F^+ \\ I_F^- \\ I_F^0 \end{bmatrix} = \frac{1}{3}\begin{bmatrix} 1 & \alpha & \alpha^2 \\ 1 & \alpha^2 & \alpha \\ 1 & 1 & 1 \end{bmatrix}\begin{bmatrix} I_{Fa} \\ 0 \\ 0 \end{bmatrix} = \frac{1}{3}\begin{bmatrix} I_{Fa} \\ I_{Fa} \\ I_{Fa} \end{bmatrix} \quad (1)$$

where all quantities are phasor quantities and $\alpha = e^{j2\pi/3}$. From this, the equation for the second set of boundary conditions can be written in the sequence domain as.

$$U_f^+ + U_f^- + U_f^0 = Z_F(I_F^+ + I_F^- + I_F^0) = 3Z_F I_F^+ \tag{2}$$

To satisfy (1) and (2), the derived sequence networks should all be connected in series at the fault terminals through the impedance, $3Z_F$. As shown in Figure 4, the sequence-domain circuit of the GFM-PGC system can be further plotted under an SLG fault.

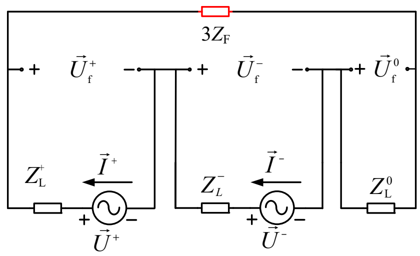

Figure 4. Sequence-domain circuit of the GFM-PGC system under an SLG fault.

Based on Figure 4, the positive- and negative-sequence current vectors of the GFM-PGC system are obtained as follows.

$$\begin{aligned} \vec{I}^{+} &= |Y_1|\angle\phi_1 \vec{U}^{+} - |Y_2|\angle\phi_2 \vec{U}_f^{+} + |Y_3|\angle\phi_3 \vec{U}_f^{-} \\ \vec{I}^{-} &= |Y_4|\angle\phi_4 \vec{U}^{-} - |Y_5|\angle\phi_5 \vec{U}_f^{-} + |Y_6|\angle\phi_6 \vec{U}_f^{+} \end{aligned} \tag{3}$$

where $\vec{U}_f^{+}$ and $\vec{U}_f^{-}$ are the positive- and negative-sequence voltage vectors of the grid at the fault point, respectively, and θ_f^+ and θ_f^- are the positive- and negative-sequence voltage phases of the grid at the fault point, respectively.

The first terms of $\vec{I}^{+}$ and $\vec{I}^{-}$ are associated with the positive- and negative-sequence machine terminal voltages. The second terms of $\vec{I}^{+}$ and $\vec{I}^{-}$ are related to the positive- and negative-sequence voltages at the fault point, respectively. The third terms of $\vec{I}^{+}$ and $\vec{I}^{-}$ are associated with the sequence coupling, which is induced by the positive- and negative-sequence voltage injection. Hence, the positive-sequence voltage at the fault point generates a component in the negative-sequence machine terminal current, and the negative-sequence voltage at the fault point generates a component in the positive-sequence machine terminal current.

The positive- and negative-sequence voltage vectors of the system are controlled in the dq^+ and dq^- rotating reference frames, respectively. The voltage and current vectors of the system are oriented through the output angle of the active power loop, and the rotating reference frames of the GFM-PGC system are shown in Figure 5.

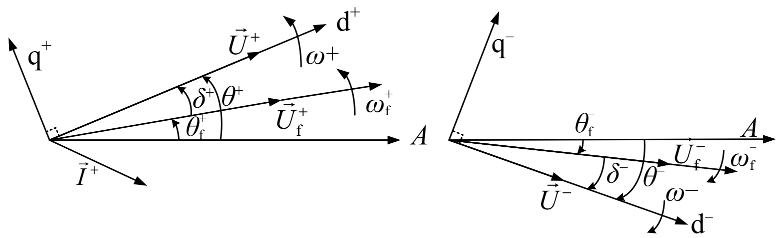

(a) Positive sequence system (b) Negative sequence system

Figure 5. Rotating reference frames of the GFM-PGC system.

Equation (3) is projected into the positive- and negative-sequence rotated reference frames using $e^{-j\theta^{+}}$ and $e^{-j\theta^{-}}$, respectively.

$$\begin{aligned} I_{d+}^{+}+jI_{q+}^{+}= &\ |Y_1|U_{d+}^{+}\angle\phi_1-|Y_2|U_f^{+}\angle(\phi_2+\theta_f^{+}-\theta^{+})+ \\ &\ |Y_3|U_f^{-}\angle(\phi_3+\theta_f^{-}-\theta^{+}) \\ I_{d-}^{-}+jI_{q-}^{-}= &\ |Y_4|U_{d-}^{-}\angle\phi_4-|Y_5|U_f^{-}\angle(\phi_5+\theta_f^{-}-\theta^{-})+ \\ &\ |Y_6|U_f^{+}\angle(\phi_6+\theta_f^{+}-\theta^{-}) \end{aligned} \tag{4}$$

According to Equation (4), the coupling between the positive- and negative-sequence systems results in a negative-sequence second harmonic frequency component (NSSHFC) in the positive-sequence current and a positive-sequence second harmonic frequency component (PSSHFC) in the negative-sequence current in the system. In order to eliminate this coupling, a notch filter is used to filter out the NSSHFC of the positive-sequence current and the PSSHFC of the negative-sequence current. Based on Figure 5, the positive- and negative-sequence q-axis voltages of the GFM-PGC system are zero at the PCC, and active power expressions are deduced as follows.

$$\begin{aligned} P^{+}= &\ (U_{d+}^{+}I_{d+}^{+}+U_{q+}^{+}I_{q+}^{+})= \\ &\ (|Y_1|U_{d+}^{+}U_{d+}^{+}\cos(\phi_1)-|Y_2|U_{d+}^{+}U_f^{+}\cos(\phi_2-\delta^{+})) \\ P^{-}= &\ (U_{d-}^{-}I_{d-}^{-}+U_{q-}^{-}I_{q-}^{-})= \\ &\ (|Y_4|U_{d-}^{-}U_{d-}^{-}\cos(\phi_4)-|Y_5|U_{d-}^{-}U_f^{-}\cos(\phi_5-\delta^{-})) \end{aligned} \tag{5}$$

where $\delta^{+}=\theta^{+}-\theta_f^{+}$ and $\delta^{-}=\theta^{-}-\theta_f^{-}$.

2.2. Control Strategy of the GFM-PGC System during Asymmetrical Faults in the Power Grid

During asymmetrical short-circuit fault periods, the GFM-PGC system should be equipped with dynamic reactive power support capability, which satisfies the requirements of the renewable energy grid code [32]. Therefore, the LVRT control scheme of the GFM-PGC system should improve the dynamic reactive power support capability of the system. Based on the control scheme, the transient synchronous stabilization issue of the GFM-PGC system is investigated. The GFM-PGC system controls the grid-connected point voltage through the *Q-V* droop loop, and the novel *Q-V* droop control scheme is shown in Equation (6).

$$\begin{cases} U^{+}=K_q^{+}(Q_{ref}^{+}-Q^{+})+U_{d+}^{+} \\ U^{-}=K_q^{-}(Q_{ref}^{-}-Q^{-})+U_{d-}^{-} \end{cases} \tag{6}$$

where U_{d+}^{+} and U_{d-}^{-} are the positive- and negative-sequence d-axis voltage components at the PCC, respectively. Combining Equation (6) and Figure 6, the control equation of the voltage loop can be further obtained as follows.

$$\begin{cases} i_{ldref}^{+}=(K_q^{+}(Q_{ref}^{+}-Q^{+}))(k_{pv}+k_{iv}/s) \\ i_{ldref}^{-}=(K_q^{-}(Q_{ref}^{-}-Q^{-}))(k_{pv}+k_{iv}/s) \end{cases} \tag{7}$$

where k_{pv} and k_{iv} are the voltage loop proportional and integral coefficients.

According to Equation (7), the difference between the reference value and the actual value of the reactive power is controlled by the PI controller of the d-axis voltage loop. And the steady-state error in the reference value and the actual value of the reactive power can be eliminated. By adopting the *Q-V* droop control structure proposed in this paper, the positive- and negative-sequence reactive power of the system can accurately follow the reference value of the reactive power. The system can inject appropriate positive- and negative-sequence reactive currents into the grid to meet the requirements of the grid code. Consequently, the system does not have to switch the control strategy during the whole fault period, and the system realizes the full process of grid-forming control. At the same time, the proposed control strategy can be applied to the normal operation and fault period of the grid without switching the control mode. In addition, this paper also proposes a negative-sequence *Q*-*V* control scheme during asymmetrical short-circuit faults. The proposed scheme solves the problem that the traditional control scheme cannot determine the reference value of the negative-sequence *Q*-*V* loop during faults.

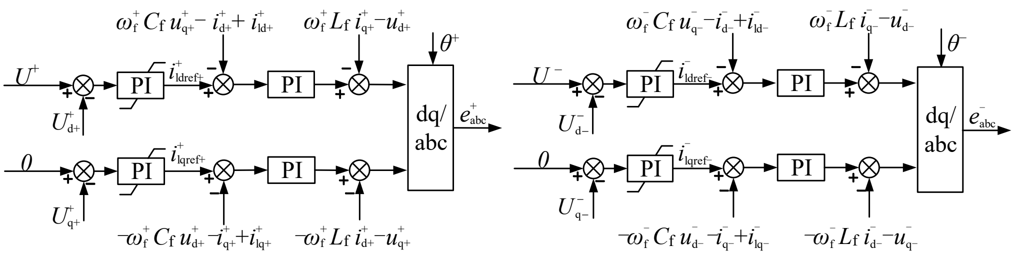

(a) Positive sequence control loop (b) Negative sequence control loop

Figure 6. Block diagrams of the voltage and current control loops of the GFM-PGC system.

In summary, block diagrams of the positive- and negative-sequence voltage and current control loops of the GFM-PGC system are shown in Figure 6a,b.

As shown in Figure 6, the positive- and negative-sequence q-axis voltages at the PCC are both given as 0. The positive- and negative-sequence q-axis voltages at the PCC are always controlled to be 0 by the PI controllers of the positive- and negative-sequence q-axis voltage loops. The output voltage vectors of the GFM-PGC always coincide with the d-axis of the synchronous rotating reference frames. In the meantime, the PI controller outputs of the system's positive- and negative-sequence dq-axis voltage loops are all set with a limit value 1.5 times the rated current value. In order to reduce the short-circuit current and avoid the voltage loop PI controller output limitation, this paper limits the fault current by reasonably setting the positive- and negative-sequence active currents of the system. The scheme can inject positive- and negative-sequence reactive currents which satisfy the requirements of the grid code, and the scheme realizes the full process of grid-forming control.

The GFM-PGC system outputs the voltage phase angle through the *P*-*f* loop. The positive- and negative-sequence system active power loop control equations are shown in Equation (8), and control block diagrams are shown in Figure 7a,b.

$$\begin{cases} J^+ \frac{d\omega^+}{dt} = P^+_{\text{ref}} - P^+ - D^+(\omega^+ - \omega^+_{\text{f}}) \\ J^- \frac{d\omega^-}{dt} = P^-_{\text{ref}} - P^- - D^-(\omega^- - \omega^-_{\text{f}}) \end{cases} \tag{8}$$

where J^+ and J^- are the positive- and negative-sequence virtual inertias of the GFM-PGC system, respectively; D^+ and D^- are the positive- and negative-sequence virtual damping coefficients; ω^+ and ω^- are the positive- and negative-sequence output angular frequencies of the system, respectively; ω^+_{f} and ω^-_{f} are the base values of the grid's positive- and negative-sequence angular frequencies; and θ^+ and θ^- are the positive- and negative-sequence voltage phase angles at the PCC.

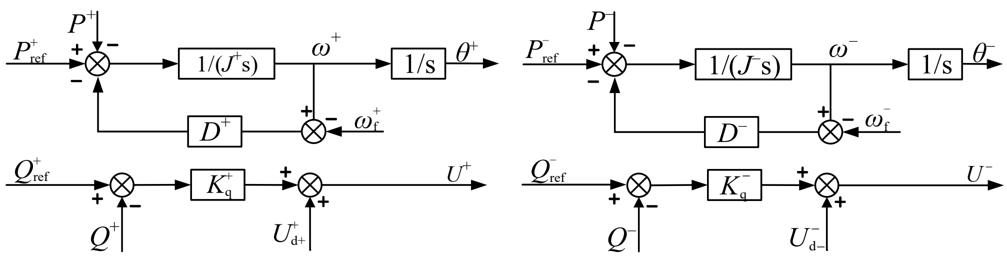

(a) Positive sequence power loop (b) Negative sequence power loop

Figure 7. Diagrams of the power control loops of the GFM-PGC system.

3. Transient Stability Analysis of the GFM-PGC System during Asymmetric Faults

During asymmetric grid fault periods, the GFM-PGC system should perform LVRT control according to the renewable energy grid code. Due to the grid voltage sag and the change in the power reference value, the system enters into a resynchronization process. This process involves the ability of the system to maintain synchronization with the grid. In order to maintain synchronized operations with the grid, the system has a stable equilibrium point (SEP), and the system is able to maintain transient synchronization stability during faults. The transient stability of the positive- and negative-sequence systems is analyzed in detail below.

3.1. Transient Synchronization Stability of the GFM-PGC Positive-Sequence System during Asymmetric Faults

When an asymmetrical short-circuit fault occurs in the grid, the GFM-PGC system should output a reactive current which meets the requirements of the grid code. The reactive current ensures that the system has dynamic reactive power support capability during LVRT. Therefore, during the fault period, the reactive power of the system should be adjusted to inject a positive-sequence reactive current which meets the requirements of the grid code. The GFM-PGC system can provide dynamic reactive power support during LVRT, and the GFM-PGC system can realize the full process of grid-forming control. When the positive-sequence PCC voltage component decreases, the positive-sequence reactive power reference (Q^+_{ref}) is given by the following equation [33].

$$Q^+_{\mathrm{ref}} = \begin{cases} 0 & \text{normal} \\ k^+(0.9 - \frac{U^+_{\mathrm{d}+}}{U_{\mathrm{N}}})U^+_{\mathrm{d}+} I_{\mathrm{N}} & \text{fault} \end{cases} \tag{9}$$

where k^+ is the dynamic positive-sequence reactive power current proportional coefficient of the GFM-PGC system, U_{N} is the rated voltage of the system and I_{N} is the rated current of the system.

The positive-sequence power-angle characteristic curve during a grid short-circuit fault is shown in Figure 8. If the curves of P^+ and P^+_{reff} do not intersect during the fault period, the GFM-PGC positive-sequence system will have no SEP. ω^+ and δ^+ will change monotonically, and the system will be transient instability. Therefore, P^+_{reff} must satisfy the following conditions.

$$\left[\max(P^+) \geq P^+_{\mathrm{reff}}\right] \cap \left[\min(P^+) \leq P^+_{\mathrm{reff}}\right] \tag{10}$$

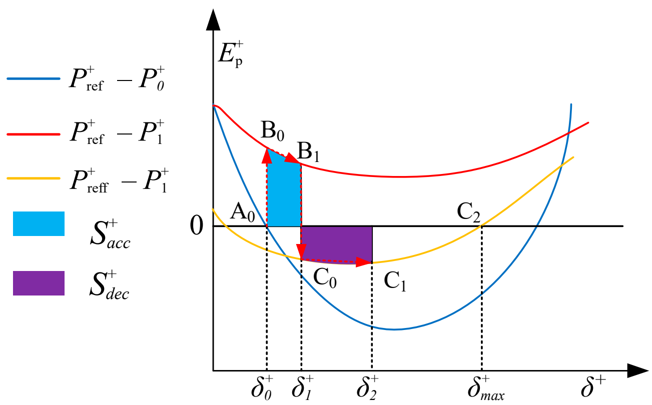

Figure 8. The trajectory of δ^+ from the prefault stage to the fault stage.

According to Equation (10), it can be determined whether the SEP of the GFM-PGC positive-sequence system exists or not. However, even if the SEP exists, the system still has the risk of instability during the transient process. By simulating the two-order rotor motion equation of the SG, the GFM-PGC system and the stand-alone infinity system have similar power-angle characteristic curves. Consequently, the transient process of the GFM-PGC system during a fault can be analyzed through the equal area criterion. According to Equation (8), the transient energy function during the fault period of the positive-sequence system can be obtained as follows.

$$\underbrace{\frac{1}{2}J^{+}(\omega^{+}-\omega_{\mathrm{f}}^{+})^{2}\Big|_{\delta_{0}^{+}}^{\delta_{\mathrm{t}}^{+}}}_{\Delta E_{\mathrm{K}}^{+}}=\underbrace{\int_{\delta_{0}^{+}}^{\delta_{\mathrm{t}}^{+}}(P_{\mathrm{ref}}^{+}-P^{+})\mathrm{d}\delta^{+}}_{\Delta E_{\mathrm{P}}^{+}}=f_{\mathrm{E}}(\delta^{+},P_{\mathrm{ref}}^{+}) \tag{11}$$

where $\Delta E_{\mathrm{K}}^{+}$ is proportional to the square of the angular frequency deviation and $\Delta E_{\mathrm{K}}^{+}$ can be defined as the variation in the equivalent kinetic energy of the positive-sequence system. $\Delta E_{\mathrm{K}}^{+}$ characterizes the motion state of ω^{+} with respect to ω_{f}^{+} during the transient process. $\Delta E_{\mathrm{P}}^{+}$ is the energy accumulation of the unbalanced power during the transient process, and $\Delta E_{\mathrm{P}}^{+}$ can be defined as the variation in the equivalent potential energy of the positive-sequence system [22]. When the effect of the damping term is ignored, the equivalent kinetic and potential energies of the system are converted to each other during the transient process. In order to deeply analyze the transient process of the GFM-PGC system during a fault, the operation trajectory of the positive-sequence system power angle was analyzed in detail, as shown in Figure 8.

In the above diagram, P_{ref}^{+} is the positive-sequence active power reference value during the prefault stage and P_{reff}^{+} is the positive-sequence active power reference value during the fault duration stage. The blue, red and yellow curves are the positive-sequence power-angle characteristic curves of the system at the prefault stage, the fault detection stage and the fault duration stage, respectively. A_0 is the initial operation point of the system. The trajectory of δ^{+} reflects the sequential switching control of the GFM-PGC system from the prefault stage to the fault stage. As shown in Figure 8, the trajectory includes the following stages.

1. During the prefault stage, the initial operation point of the GFM-PGC system is A_0. When an asymmetrical fault occurs in the grid, the system enters the fault detection stage, where δ^{+} and ω^{+} remain unchanged and the operation point moves to B_0.
2. During the fault detection stage, the active power reference value of point B_0 remains P_{ref}^{+}, and $P_{\mathrm{ref}}^{+} > P^{+}$. According to Equation (8), ω^{+} continues to rise and δ^{+} moves from δ_{0}^{+} to δ_{1}^{+}. The increase in kinetic energy in the system is the acceleration area.

$$S_{\mathrm{acc}}^{+}=f_{\mathrm{E}}(\delta_{1}^{+},P_{\mathrm{ref}}^{+})-f_{\mathrm{E}}(\delta_{0}^{+},P_{\mathrm{ref}}^{+}) \tag{12}$$

3. The GFM-PGC system detects an asymmetrical fault in the grid. To ensure that there is an SEP during the transient process of the system, the range of active power reference values is determined based on Equation (10). δ^{+} and ω^{+} remain unchanged, and the operation point moves from B_1 to C_0.
4. The active power reference value at point C_0 is P_{reff}^{+}, and $P_{\mathrm{reff}}^{+} < P^{+}$. Based on Equation (8), ω^{+} continues to decrease, and δ^{+} increases until ω^{+} decreases to ω_{f}^{+}. δ^{+} rises from δ_{1}^{+} to δ_{2}^{+}. The reduction in kinetic energy in the system is the deceleration area.

$$S_{\mathrm{dec}}^{+}=f_{\mathrm{E}}(\delta_{1}^{+},P_{\mathrm{reff}}^{+})-f_{\mathrm{E}}(\delta_{2}^{+},P_{\mathrm{reff}}^{+}) \tag{13}$$

As shown in Figure 8, when the operation point moves to C_2, δ^{+} is equal to $\delta_{\mathrm{max}}^{+}$. If ω^{+} is still larger than ω_{f}^{+}, δ^{+} continues to increase, and $P_{\mathrm{reff}}^{+} > P^{+}$. According to Equation (8), ω^{+} continues to rise, and δ^{+} continues to increase. The system will experience transient instability. To obtain the critical clearance angle (δ_{cr}^{+}), let $\delta_{2}^{+} = \delta_{\mathrm{max}}^{+}$, where $\delta_{\mathrm{max}}^{+}$ is the right intersection of P_{1}^{+} and P_{reff}^{+}. Hence, the transient synchronous stability criterion of the positive-sequence system from the prefault stage to the fault stage can be obtained as follows [22].

$$\begin{cases} S_{\text{acc}}^{+} < S_{\text{dec}}^{+} + \Delta E_{D}^{+} \\ \Delta E_{D}^{+} = \int_{\delta_0^{+}}^{\delta_{\max}^{+}} D^{+} \mathrm{d}\delta^{+} \end{cases} \tag{14}$$

According to Equation (14), as the acceleration area of the positive-sequence system increases, the kinetic energy accumulated in the transient process will increase, which is detrimental to the stable operation of the system. Meanwhile, a smaller positive-sequence damping coefficient will lead to a decrease in the damping area during the transient period, which will deteriorate the transient stability of the GFM-PGC system.

3.2. Transient Synchronization Stability of the GFM-PGC Negative-Sequence System during Asymmetric Faults

When an asymmetrical short-circuit fault occurs in the grid, the GFM-PGC system should absorb negative-sequence dynamic reactive current from the grid to suppress the negative-sequence voltage rise [33]. By adjusting the negative-sequence reactive power reference value during the fault, the system can absorb the appropriate negative-sequence reactive current from the grid. The negative-sequence reactive power reference (Q_{ref}^{-}) is shown below [33].

$$Q_{\text{ref}}^{-} = \begin{cases} 0 & \text{normal} \\ k^{-} \frac{U_{\text{d}-}^{-}}{U_{\text{N}}} U_{\text{d}-}^{-} I_{\text{N}} & \text{fault} \end{cases} \tag{15}$$

where k^{-} is the dynamic negative-sequence reactive current proportional coefficient of the GFM-PGC system.

The negative-sequence power-angle characteristic curve during a grid short-circuit fault is shown in Figure 9. If the curves of P^{-} and P_{ref}^{-} do not intersect during the fault stage, the GFM-PGC negative-sequence system will have no SEP. ω^{-} and δ^{-} will change monotonically, and the system will be destabilized. Therefore, P_{ref}^{-} must satisfy the following equation.

$$\left[\max(P^{-}) \geq P_{\text{ref}}^{-}\right] \cap \left[\min(P^{-}) \leq P_{\text{ref}}^{-}\right] \tag{16}$$

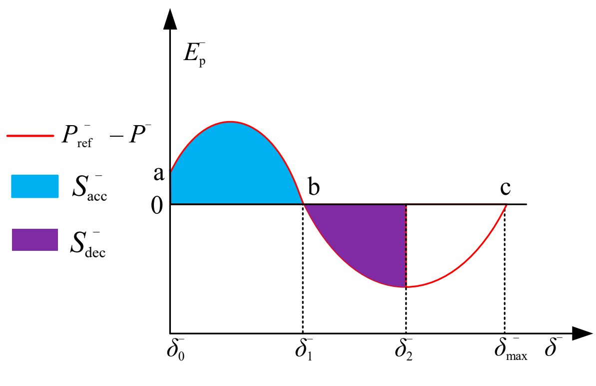

Figure 9. The trajectory of δ^{-} from the prefault stage to the fault stage.

According to Equation (16), it can be determined whether there is an SEP in the GFM-PGC negative-sequence system. Similarly, the conversion process of equivalent kinetic energy and potential energy of the GFM-PGC negative-sequence system can be analyzed through the equal area criterion during the fault period. According to Equation (8), the transient energy function of the negative-sequence system can be obtained as follows.

$$\underbrace{\frac{1}{2} J^{-} (\omega^{-} - \omega_{\text{f}}^{-})^2 \Big|_{\delta_0^{-}}^{\delta_{\text{t}}^{-}}}_{\Delta E_{\text{K}}^{-}} = \underbrace{\int_{\delta_0^{-}}^{\delta_{\text{t}}^{-}} (P_{\text{ref}}^{-} - P^{-}) \mathrm{d}\delta^{-}}_{\Delta E_{\text{P}}^{-}} = f_{\text{E}}(\delta^{-}, P_{\text{ref}}^{-}) \tag{17}$$

Similar to the positive-sequence system, ΔE_{K}^{-} can be defined as the variation in the equivalent kinetic energy of the negative-sequence system. ΔE_{P}^{-} can be defined as the variation in the equivalent potential energy of the negative-sequence system. The trajectory of the GFM-PGC negative-sequence system power angle from the prefault stage to the fault stage is shown in Figure 9.

In the above diagram, P^-_{ref} is the active power reference value of the negative sequence. The red curve is the negative-sequence power-angle characteristic curve of the system during the fault stage. Similar to the transient process of the positive-sequence system, the trajectory of δ^- can reflect the transient process of the negative-sequence system. It is shown in Figure 9. The trajectory includes the following stages.

1. During the prefault stage, the initial operation point of the GFM-PGC system is the coordinate origin. When an asymmetrical fault occurs in the grid, δ^- and ω^- remain unchanged and the operation point will be shifted to a, where δ^-_0 has an initial value of zero.
2. During the fault duration stage, $P^-_{\text{ref}} = 0$. According to Equation (8), ω^- continues to rise, and δ^- moves from δ^-_0 to δ^-_1. The increase in the kinetic energy in the system is the acceleration area.
$$S^-_{\text{acc}} = f_{\text{E}}(\delta^-_1, P^-_{\text{ref}}) - f_{\text{E}}(\delta^-_0, P^-_{\text{ref}}) \tag{18}$$
3. The operation point of the system moves to b and the downward motion continues; in the meantime, the active power reference $P^-_{\text{ref}} < P^-$. Based on Equation (8), ω^- continues to decrease. δ^- continues to increase until ω^- decreases to ω^-_{f}. δ^- moves from δ^-_1 and rises to δ^-_2. And the reduction in the kinetic energy in the system is the deceleration area.
$$S^-_{\text{dec}} = f_{\text{E}}(\delta^-_1, P^-_{\text{ref}}) - f_{\text{E}}(\delta^-_2, P^-_{\text{ref}}) \tag{19}$$

As shown in Figure 9, when the operation point moves to c, $\delta^- = \delta^-_{\text{max}}$. If ω^- is still greater than ω^-_{f}, δ^- continues to increase, and $P^-_{\text{ref}} > P^-$. According to Equation (8), ω^- and δ^- continues to rise, and the system will eventually destabilize. To obtain the maximum deceleration area, let $\delta^-_2 = \delta^-_{\text{max}}$, where δ^-_2 is the right-hand intersection of P^- and P^-_{ref}. Therefore, the transient synchronous stability criterion of the negative-sequence system from the prefault stage to the fault stage can be obtained as follows.

$$\begin{cases} S^-_{\text{acc}} < S^-_{\text{dec}} + \Delta E^-_D \\ \Delta E^-_D = \int_{\delta^-_0}^{\delta^-_{\text{max}}} D^- \text{d}\delta^- \end{cases} \tag{20}$$

4. Simulation Verification

According to the main circuit structure of the GFM-PGC system shown in Figure 1 and the control structure shown in Figure 7, a simulation model of a 2 MW GFM-PGC system was built in Matlab/Simulink (2021b). The simulation results validated the effectiveness of the proposed *Q-V* droop control strategy of the GFM-PGC system. The correctness of the transient stability criterion of the system was also verified under grid asymmetrical short-circuit fault conditions. The parameters of the simulation model are shown in Table 1.

Table 1. The parameters of the simulation model.

Symbol	Value	Symbol	Value
S_N	2 MW	Z_L	0.115 + j0.264 p.u.
U_N	690 V	Z_g	1×10^{-5} + j 1×10^{-6} p.u.
J^+	60 kg·m^2	D^+	25
J^-	50 kg·m^2	D^-	40
K_q^+	0.05	K_q^-	0.03
L_f	0.13 p.u.	R_f	0.013 p.u.
C_f	0.075 p.u.	ω	100π rad/s
K_{pv}^+, K_{iv}^+	10, 800	K_{pi}^+, K_{ii}^+	1, 10
K_{pv}^-, K_{iv}^-	40, 600	K_{pv}^-, K_{ii}^-	0.05, 0.5

4.1. Validation of the Transient Stability Criterion for the GFM-PGC Positive-Sequence System

The simulated working conditions of the GFM-PGC positive-sequence system when an asymmetric short-circuit fault occurs are shown in Table 2.

Table 2. Simulation and verification of GFM-PGC positive-sequence system.

Case	P^+_{reff}	D^+	$U^+_{\text{d+}}$	S^+_{acc}	$S^+_{\text{dec}} + \Delta E^+_{\text{D}}$	Stability
1	0.5 p.u.	25	0.71	0.154	0.169	Stable
2	0.5 p.u.	7	0.71	0.154	0.140	Unstable
3	0.5 p.u.	20	0.40	0.163	0.147	Unstable
4	0.5 p.u.	20	0.71	0.154	0.159	Stable

In Case 1 and Case 2, the effect of the positive-sequence damping coefficient on the transient stability of the GFM-PGC system was investigated. During the normal operation of the grid, the GFM-PGC system adopts the outer power loop and the inner voltage current double-loop control mode. P^+_{ref} and Q^+_{ref} were set to 1 p.u. and 0 p.u., respectively. In Figure 10, P^+ and Q^+ are 1 p.u. and 0 p.u., which indicates that the active and reactive powers can accurately follow the reference values. During the fault duration stage, P^+_{reff} is set to 0.5 p.u. in order to make the system exist at an SEP. Q^+_{ref} is set to 0.27 p.u., according to Equation (9). D^+ is equal to 25 in Case 1, and the detection delay of the system t_{d} = 40 ms. According to Equations (12) and (13), $S^+_{\text{acc}} < S^+_{\text{dec}} + E_D{}^+$, which satisfies the transient stability criterion (Equation (14)). The GFM-PGC system output power values, P^+ and Q^+, are 0.5 p.u. and 0.27 p.u. during the fault period, which indicates that P^+ and Q^+ can follow the reference values quickly. The system remains stable during the fault period. In Case 2, D^+ is set to 7 and $S^+_{\text{acc}} > S^+_{\text{dec}} + E_D{}^+$. The kinetic energy accumulated by the GFM-PGC system during acceleration cannot be released at the deceleration stage. The excess kinetic energy will drive the GFM-PGC system to cross the transient instability boundary, which will lead to system transient instability. As shown in Figure 10, the system output power values, P^+ and Q^+, fluctuate significantly. The system frequency is greater than the rated frequency, and the system frequency and the power angle oscillate continuously. The correctness of the theoretical derivation was verified by simulations.

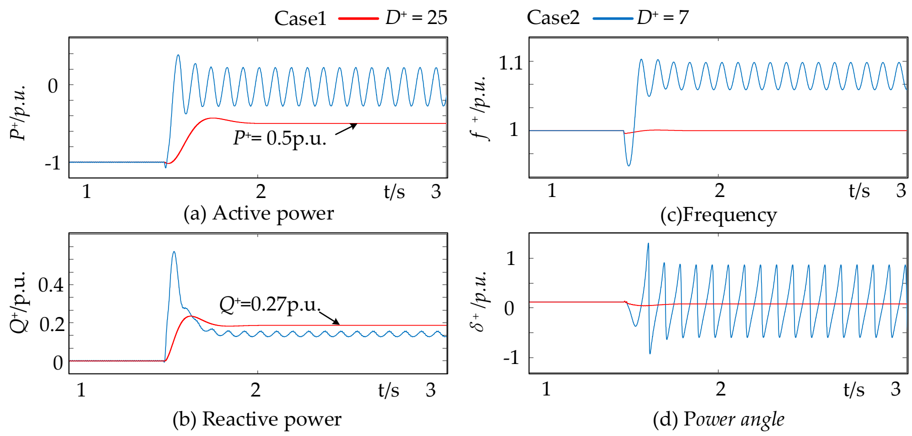

Figure 10. The simulation waveforms of the GFM-PGC system with different D^+ values.

In Case 3 and Case 4, the effect of the voltage drop degree on the transient stability of the GFM-PGC system was investigated. During the fault duration stage, P^+_{reff} was set to 0.5 p.u. in order to make the system exist at an SEP. Meanwhile, the PCC voltage $U^+_{\text{d+}}$ = 0.40 p.u. Q^+_{ref} was set to 0.4 p.u. according to Equation (9). D^+ was equal to 20 in Case 3. According to Equations (12) and (13), $S^+_{\text{acc}} > S^+_{\text{dec}} + E_D{}^+$, which does not satisfy the transient stability criterion (Equation (14)). As shown in Figure 11, the system output power values, P^+ and Q^+, fluctuate significantly. The system frequency and power angle oscillate continuously. In Case 4, the PCC voltage $U^+_{\text{d+}}$ = 0.71 p.u., and Q^+_{ref} is set to 0.27 p.u. P^+_{reff} is set to 0.5 p.u., and D^+ is set to 20. According to Equations (12) and (13), $S^+_{acc} < S^+_{dec} + E_D{}^+$, which satisfies the transient stability criterion (Equation (14)). As shown in Figure 11, The GFM-PGC system output power values, P^+ and Q^+, are 0.5 p.u. and 0.27 p.u. during the fault period, which indicates that P^+ and Q^+ can follow the reference values quickly. The system remains stable during the fault period. With the decrease in the grid voltage drop, the equivalent acceleration area of the system decreases, the equivalent deceleration area increases and the system will be more stable. At the same time, the frequency overshoot of the system is reduced, and the stable state can be reached faster.

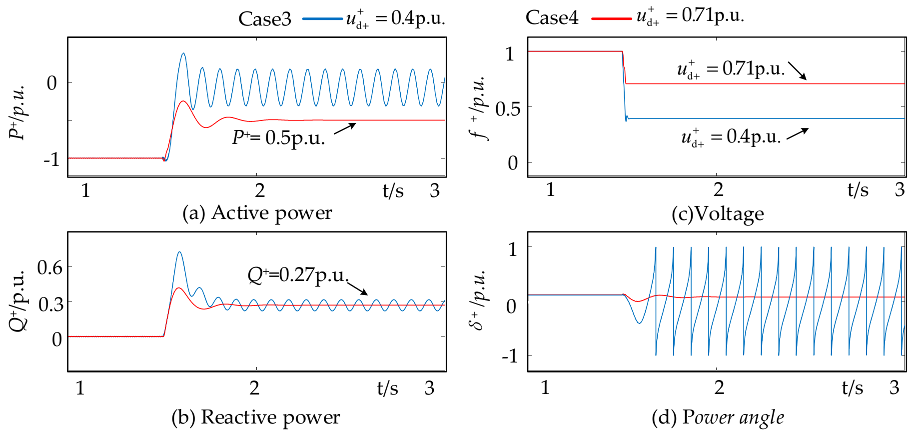

Figure 11. The simulation waveforms of the GFM-PGC system with different U^+_{d+} values.

4.2. Validation of the Transient Stability Criterion for the GFM-PGC Negative-Sequence System

In Case 5 and Case 6, the transient stability of the GFM-PGC negative-sequence system during asymmetrical faults was investigated. In Figure 12, the grid operates normally, and the A-phase grid voltage drops to 0 p.u. at 1.5 s. During normal grid operation, the GFM-PGC system uses the outer power loop and the voltage current double-loop mode. P^-_{ref} and Q^-_{ref} are both set to 0 p.u. During the fault duration stage, P^-_{ref} is set to 0 p.u. Meanwhile, the PCC voltage U^-_{d-} is equal to 0.28 p.u. According to Equation (15), the reactive power reference (Q^-_{ref}) is -0.16 p.u. According to Equations (18) and (19), $S^-_{acc} < S^-_{dec} + E_D{}^-$. Meanwhile, the GFM-PGC system's P^- and Q^- values are 0 p.u. and -0.16 p.u., which indicates that P^- and Q^- can follow the reference values quickly. The system will remain stable. In Case 6, the negative-sequence damping coefficient (D^-) is set to 10. Based on Equations (18) and (19), $S^-_{acc} > S^-_{dec} + E_D{}^-$. And the system will cross the unstable equilibrium point (UEP), and a transient instability phenomenon will occur. As shown in Figure 12, the output power of the GFM-PGC system (P^- and Q^-) fluctuates significantly. The system frequency and power angle oscillate continuously.

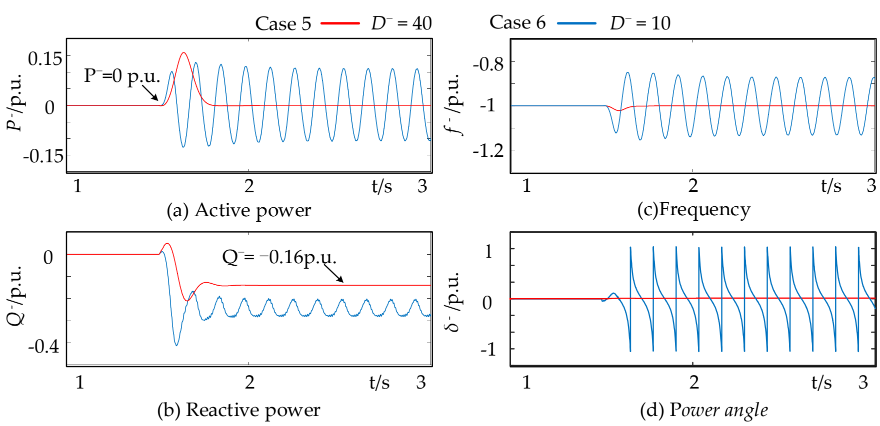

Figure 12. Simulation and verification of the GFM-PGC negative-sequence system.

Table 3 shows the transient calculation results of the simulation conditions described above.

Table 3. Simulation and verification of the GFM-PGC negative-sequence system.

Case	D^-	S^-_{acc}	$S^-_{dec} + \Delta E^-_D$	Stability
5	40	0.422	0.584	Stable
6	10	0.422	0.331	Unstable

5. Experimental Verification

In order to further verify the correctness of the transient stability criterion of the GFM-PGC system proposed in this paper, the hardware-in-the-loop experimental platform shown in Figure 13 was constructed. The main circuit of the GFM-PGC system is simulated by a semi-physical real-time simulator, and the grid-connected inverters are real-time controlled by the core control board of the DSP+FPGA. The specific experimental parameters are the same as in Table 1.

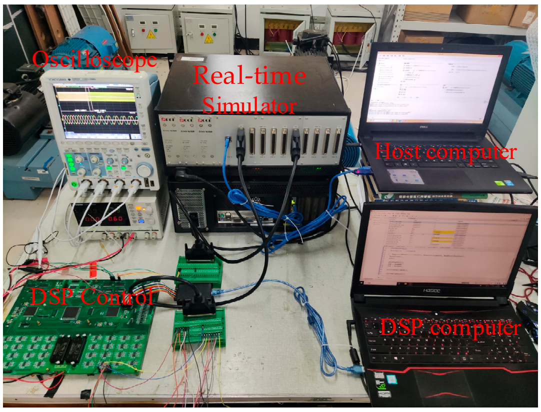

Figure 13. Hardware-in-the-loop experimental platform.

5.1. Experimental Validation of the Transient Stability Criterion for the GFM-PGC Positive-Sequence System

The experimental working conditions of the GFM-PGC positive-sequence system are shown in Table 4.

Table 4. Experimental verification of the GFM-PGC positive-sequence system.

Case	P^+_{reff}	U^+_{d+}	D^+	S^+_{acc}	$S^+_{dec} + \Delta E^+_D$	Stability
1	0.5	0.71	25	0.235	0.327	Stable
2	0.5	0.71	40	0.235	0.359	Stable
3	0.5	0.80	25	0.167	0.378	Stable
4	0.68	0.71	25	0.235	0.189	Unstable

The effect of the damping coefficient on the transient stability of the GFM-PGC system was investigated in Case 1 and Case 2. During the normal operation of the grid, the GFM-PGC system adopts the outer power loop and the inner voltage current double-loop control mode. P^+_{ref} and Q^+_{ref} is set to 1 p.u. and 0 p.u. As shown in Figure 14, the P^+ and Q^+ values are 1 p.u. and 0 p.u., which indicates that the active and reactive powers can accurately follow the reference values. In Case 1, the positive-sequence voltage at PCC drops to 0.71 p.u. at 1.5 s. P^+_{reff} is set to 0.5 p.u., and D^+ is set to 25. The reactive power reference (Q^+_{ref}) is set to 0.27 p.u., according to Equation (9). On the basis of Equation (12), S^+_{acc} = 0.235. And the sum of the maximum deceleration area and the damping area S^+_{dec} + $E_D{}^+$ = 0.327, which satisfies the transient stability criterion (Equation (14)). As shown in Figure 14, the P^+ and Q^+ values of the GFM-PGC system are 0.5 p.u. and 0.27 p.u., respectively, which shows that they can follow the reference values quickly. The system can remain stable during the fault.

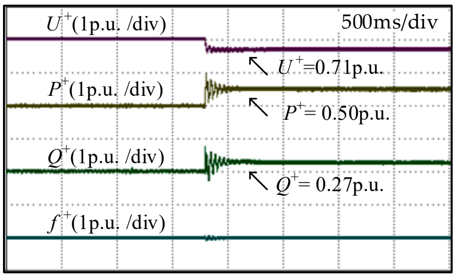

Figure 14. The experimental waveforms of the GFM-PGC system when D^+ = 25.

In Case 2, the positive-sequence voltage at the PCC dropped to 0.71 p.u. at 1.5 s. P^+_{reff} was set to 0.5 p.u., and the damping coefficient D^+ was set to 40. The reactive power reference (Q^+_{ref}) was 0.27 p.u., based on the grid code. According to Equations (12) and (13), S^+_{acc} = 0.235 and S^+_{dec} + $E_D{}^+$ = 0.359, which satisfies the transient stability criterion (Equation (14)). As shown in Figure 15, the output power values, P^+ and Q^+, of the GFM-PGC system are 0.5 p.u. and 0.27 p.u., which indicates that P^+ and Q^+ can quickly follow the reference values and that the system reaches stability. As the positive-sequence damping coefficient increases, the GFM-PGC system will consume more equivalent kinetic energy during transients, and the system will be more stable.

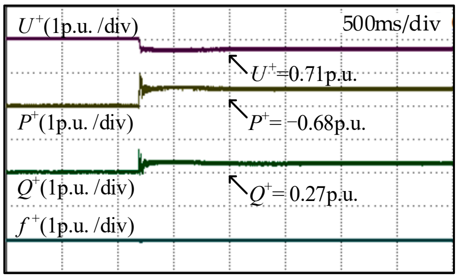

Figure 15. The experimental waveforms of the GFM-PGC system when D^+ = 40.

In Case 3, the effect of the degree of voltage sag on the transient stability of the GFM-PGC system was investigated. The positive-sequence voltage dropped to 0.80 p.u. at 1.5 s. P^+_{reff} was set to 0.5 p.u., and the damping coefficient (D^+) was set to 25. The reactive power reference (Q^+_{ref}) was 0.16 p.u. According to Equation (12), S^+_{acc} = 0.167 and S^+_{dec} + $E_D{}^+$ = 0.378, which satisfies the transient stability criterion (Equation (14)). As shown in Figure 16, the P^+ and Q^+ values of the GFM-PGC system are 0.5 p.u. and 0.16 p.u., respectively, which shows that they can follow the reference values quickly. Meanwhile, the system frequency overshoot decreases, and the system frequency can reach the steady state faster. As the degree of voltage sag decreases, the equivalent acceleration area of the system decreases and the equivalent deceleration area increases. The system will be more stable.

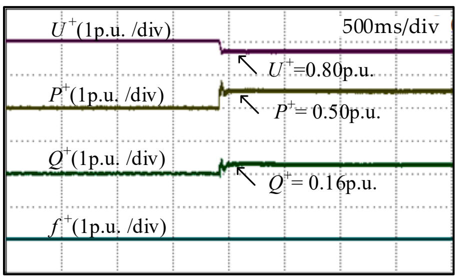

Figure 16. The experimental waveform of the GFM-PGC system when the voltage drops to 0.80 p.u.

In Case 4, the effect of the active power reference value on the transient stability of the GFM-PGC system was investigated. The positive-sequence voltage dropped to 0.71 p.u. at 1.5 s. During the fault duration stage, the active power reference value (P^+_{reff}) of the GFM-PGC system was set to 0.68 p.u., and the damping coefficient (D^+) was set to 25. The reactive power reference (Q^+_{ref}) was 0.27 p.u., based on Equation (9). According to Equations (12) and (13), S^+_{acc} = 0.235 and S^+_{dec} + $E_{\mathrm{D}}{}^+$ = 0.189, which does not satisfy the transient stability criterion (Equation (14)). As shown in Figure 17, the system output power values, P^+ and Q^+, fluctuate significantly. As P^+_{reff} becomes larger, the maximum equivalent deceleration area of the system decreases, and the system becomes less stable.

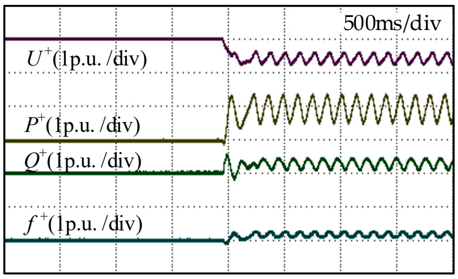

Figure 17. The experimental waveforms of the GFM-PGC system when P^+_{reff} = 0.68 p.u.

5.2. Experimental Validation of Transient Stability Criterion for the GFM-PGC Negative-Sequence System

The experimental working conditions of the GFM-PGC negative-sequence system are shown in Table 5.

Table 5. Experimental verification of the GFM-PGC negative-sequence system.

Case	D^-	S^-_{acc}	$S^-_{\mathrm{dec}} + \Delta E^-_{\mathrm{D}}$	Stability
5	40	0.423	0.582	Stable
6	8	0.423	0.316	Unstable

The transient stability of the GFM-PGC negative-sequence system during asymmetrical faults was investigated in Case 5 and Case 6. The grid operates normally and an SLG fault occurs at 2 s, which causes the A-phase grid voltage to drop to 0 p.u. During normal grid operation, the GFM-PGC system uses the outer power loop and the voltage current dual-loop control modes. Meanwhile, P^-_{ref} and Q^-_{ref} are both set to 0 p.u. During the fault duration stage, the active power reference value (P^-_{ref}) of the GFM-PGC system was set to 0 p.u., and the damping coefficient D^- was set to 40. The reactive power reference (Q^-_{ref}) was −0.16 p.u., according to Equation (15). According to Equations (18) and (19), $S^-_{\mathrm{acc}} < S^-_{\mathrm{dec}} + \mathrm{E_D}^-$. As shown in Figure 18, the system's P^- and Q^- values are 0 p.u. and −0.16 p.u., respectively. P^- and Q^- can follow the reference values quickly, and the system can reach the steady state.

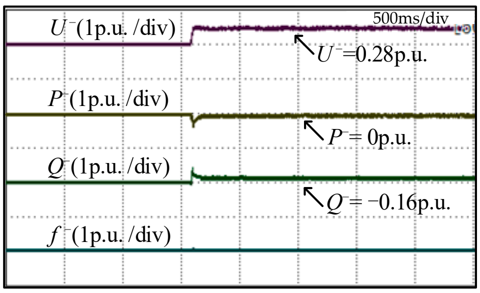

Figure 18. The experimental waveforms of the GFM-PGC system when D^- = 40.

In Case 6, an SLG fault occurs at 2 s. During the fault duration stage, the active power reference value (P^-_{ref}) of the GFM-PGC system was set to 0 p.u., and the damping coefficient D^- was set to 8. The reactive power reference value Q^-_{ref} was −0.16 p.u., according to Equation (15). On the basis of Equations (18) and (19), $S^-_{acc} > S^-_{dec} + E_D{}^-$. As shown in Figure 19, the output power values, P^- and Q^-, of the GFM-PGC system will fluctuate significantly and the system will be unstable.

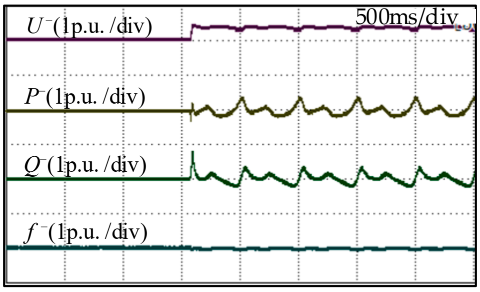

Figure 19. The experimental waveforms of the GFM-PGC system when D^- = 8.

According to the above simulations and experiments, it can be seen that during a grid short-circuit fault, the positive- and negative-sequence reactive currents that satisfy the requirements of the grid code should be injected preferentially. By reasonably regulating the positive- and negative-sequence active currents of the system, the system will not trigger current limitation. The inner voltage loop of the system is controlled during the entire fault period. Therefore, the transient stability criterion in this paper has good applicability.

6. Conclusions

In this paper, a mathematical model of the GFM-PGC system under asymmetrical short-circuit faults in the grid is established, and a novel *Q*-*V* control strategy for the GFM-PGC is proposed. The transient synchronization mechanism of the system is portrayed by deriving the equations of the power angle during LVRT. On this basis, the paper analyzes synchronization characteristics such as system damping. The main conclusions are as follows.

- A novel Q-V control scheme is proposed under asymmetrical short-circuit faults. The scheme injects suitable positive- and negative-sequence reactive currents into the grid by changing the power reference value during the fault. Therefore, the GFM-PGC system does not need to switch the control strategy during the LVRT, and the system realizes the full process of grid-forming control.
- The GFM-PGC system model with positive- and negative-sequence voltages and current double-loops is established under conditions of asymmetrical short-circuit faults in the power grid. On this basis, the equivalent power-angle characteristic equations of the positive- and negative-sequence systems are derived. Considering the equilibrium point constraints of the GFM-PGC system during LVRT, the controllable operation region of the active power reference value is obtained. The synchronization mechanism and instability pattern of the GFM-PGC are illustrated by the equivalent power-angle operation trajectory diagram and equal area criterion. Corresponding positive- and negative-sequence transient stability criteria are proposed.
- The control parameters and operating states of the GFM-PGC system affect the system output characteristics. The grid voltage drop reduces the stable operation area and deteriorates the transient synchronization stability of the system. The increase in the damping coefficient and the decrease in the system output active power command value are beneficial to increase the equivalent deceleration area, which improves the transient stability of the GFM-PGC system. Finally, the correctness of the theoretical analysis is fully validated by detailed simulations and experimental results.

There are still some aspects of this paper that need further consideration and improvement. The transient synchronization stability of GFM-PGCs is discussed in this paper, but the form of multi-GFM-PGCs is usually adopted in renewable energy power generation bases. The coupling mechanism and transient synchronization stability of the multi-GFM-PGC can be further investigated considering the dynamic interaction between multi-GFM-PGC systems.

Author Contributions: Conceptualization, W.H. and J.Y.; methodology, J.Y. and Q.Z.; software, W.H. and Q.Z.; validation, X.L. and Y.L.; formal analysis, Q.Z. and J.Y.; investigation, H.X. and J.Y.; resources, X.L. and J.Y.; data curation, H.X. and Y.L.; writing—original draft preparation, W.H. and H.X.; writing—review and editing, W.H. and J.Y.; visualization, Y.L. and R.X.; supervision, X.L. and R.X.; project administration, J.Y.; funding acquisition, R.X. All authors have read and agreed to the published version of the manuscript.

Funding: This research was supported in part by the Science and Technology Project of the State Grid Chongqing Electric Power Company under grant 522023230008.

Data Availability Statement: Data are contained within the article.

Conflicts of Interest: The authors declare that this study received funding from the Science and Technology Project of the State Grid Chongqing Electric Power Company under grant 522023230008. The funder had the following involvement with the study: resources, data curation and visualization.

References

1. Ebrahim, M.A.; Ward, S.A.; El-Gohary, M.F.; Mohamad, M.A.; Eid, M.M.; Alharbi, A.H.; Khafaga, D.S. AI-based Voltage and Power Quality Control of High-penetration Grid-connected Photovoltaic Power Plant. *Front. Energy Res.* **2023**, *11*, 1178521. [CrossRef]
2. Darwish, M.M.F.; Samy, A.; Abbas, A.A.; Mansour, D.-E.A.; Ward, S.A. Impact of On-grid Photovoltaic System on Thermal Performance of the Oil-filled Transformers. In Proceedings of the 2022 23rd International Middle East Power Systems Conference (MEPCON), Cairo, Egypt, 13–15 December 2022; pp. 1–5.
3. Moulichon, A.; Alamir, M.; Debusschere, V.; Garbuio, L.; Hadjsaid, N. Polymorphic Virtual Synchronous Generator: An Advanced Controller for Smart Inverters. *Energies* **2023**, *16*, 7075. [CrossRef]
4. Xiong, X.; Wu, C.; Blaabjerg, F. An Improved Synchronization Stability Method of Virtual Synchronous Generators Based on Frequency Feedforward on Reactive Power Control Loop. *IEEE Trans. Power Electron.* **2021**, *36*, 9136–9148. [CrossRef]
5. Qu, Z.; Peng, J.C.-H.; Yang, H.; Srinivasan, D. Modeling and Analysis of Inner Controls Effects on Damping and Synchronizing Torque Components in VSG-Controlled Converter. *IEEE Trans. Energy Convers.* **2021**, *36*, 488–499. [CrossRef]
6. Pattabiraman, D.; Lasseter, R.H.; Jahns, T.M. Comparison of Grid Following and Grid Forming Control for a High Inverter Penetration Power System. In Proceedings of the 2018 IEEE Power & Energy Society General Meeting (PESGM), Portland, OR, USA, 5–10 August 2018; pp. 1–5.
7. Yazdani, S.; Ferdowsi, M.; Davari, M.; Shamsi, P. Advanced Current-Limiting and Power-Sharing Control in a PV-Based Grid-Forming Inverter Under Unbalanced Grid Conditions. *IEEE J. Emerg. Sel. Topics Power Electron.* **2020**, *8*, 1084–1096. [CrossRef]
8. Abbas, A.A.; Samy, A.; Ward, S.A.; Mansour, D.-E.A.; Darwish, M.M.F. Influence of Thermal Performance of Oil-filled Transformer on Size Limitation of Ongrid PV System. In Proceedings of the Delta University International Engineering Conference on Research and Innovation, Cairo, Egypt, 27 November 2022.
9. Debdouche, N.; Deffaf, B.; Benbouhenni, H.; Laid, Z.; Mosaad, M.I. Direct Power Control for Three-Level Multifunctional Voltage Source Inverter of PV Systems Using a Simplified Super-Twisting Algorithm. *Energies* **2023**, *16*, 4103. [CrossRef]
10. Zeb, K.; Nazir, M.S.; Ahmad, I.; Uddin, W.; Kim, H.-J. Control of Transformerless Inverter-Based Two-Stage Grid-Connected Photovoltaic System Using Adaptive-PI and Adaptive Sliding Mode Controllers. *Energies* **2021**, *14*, 2546. [CrossRef]
11. Lu, H.; Xiao, X.; Tang, G.; Lin, Z.; He, Z.; Gao, C. A Grid-forming Control Method of Modular Multilevel Converter with Integrated Distributed Photovoltaic and Battery Energy Storage System. In Proceedings of the 2023 IEEE/IAS Industrial and Commercial Power System Asia (I&CPS Asia), Chongqing, China, 7–9 July 2023; pp. 1377–1385.
12. Tozak, M.; Taskin, S.; Sengor, I. Performance Analysis of Grid Forming Converters for a Didactic Smart Grid System. In Proceedings of the 2022 57th International Universities Power Engineering Conference (UPEC), Istanbul, Turkey, 30 August–2 September 2022; pp. 1–6.
13. Ge, P.; Tu, C.; Xiao, F.; Guo, Q.; Gao, J. Design-Oriented Analysis and Transient Stability Enhancement Control for a Virtual Synchronous Generator. *IEEE Trans. Ind. Electron.* **2023**, *70*, 2675–2684. [CrossRef]
14. Singh, S.; Gao, D.W. Improved Virtual Synchronous Generator Principle for Better Economic Dispatch and Stability in Grid-Connected Microgrids with Low Noise. *Energies* **2023**, *16*, 4670. [CrossRef]
15. Ma, S.; Geng, H.; Liu, L.; Yang, G.; Pal, B.C. Grid-Synchronization Stability Improvement of Large Scale Wind Farm during Severe Grid Fault. *IEEE Trans. Power Syst.* **2018**, *33*, 216–226. [CrossRef]

16. He, X.; Pan, S.; Geng, H. Transient Stability of Hybrid Power Systems Dominated by Different Types of Grid-Forming Devices. *IEEE Trans. Energy Convers.* **2022**, *37*, 868–879. [CrossRef]
17. Taul, G.M.; Wang, X.; Davari, P.; Blaabjerg, F. Current Reference Generation Based on Next-Generation Grid Code Requirements of Grid-Tied Converters During Asymmetrical Faults. *IEEE J. Emerg. Sel. Topics Power Electron.* **2020**, *8*, 3784–3797. [CrossRef]
18. Wang, S.; Xie, Y. Virtual Synchronous Generator (VSG) Control Strategy Based on Improved Damping and Angular Frequency Deviation Feedforward. *Energies* **2023**, *16*, 5635. [CrossRef]
19. He, X.; He, C.; Pan, S.; Geng, H.; Liu, F. Synchronization Instability of Inverter-Based Generation During Asymmetrical Grid Faults. *IEEE Trans. Power Syst.* **2022**, *37*, 1018–1031. [CrossRef]
20. Fu, X. Large-Signal Stability of Grid-Forming and Grid-Following Controls in Voltage Source Converter: A Comparative Study. *IEEE Trans. Power Electron.* **2021**, *36*, 7832–7840. [CrossRef]
21. Zhang, Y.; Zhang, C.; Yang, R.; Molinas, M.; Cai, X. Current-Constrained Power-Angle Characterization Method for Transient Stability Analysis of Grid-Forming Voltage Source Converters. *IEEE Trans. Energy Convers.* **2023**, *38*, 1338–1349. [CrossRef]
22. Pei, J.; Yao, J.; Liu, Y.; Chen, S.; Sun, P.; Huang, S. Modeling and Transient Synchronization Stability Analysis for PLL-Based Renewable Energy Generator Considering Sequential Switching Schemes. *IEEE Trans. Power Electron.* **2022**, *37*, 2165–2179.
23. Liu, H.; Yang, B.; Xu, S.; Du, M.; Lu, S. Universal Virtual Synchronous Generator Based on Extended Virtual Inertia to Enhance Power and Frequency Response. *Energies* **2023**, *16*, 2983. [CrossRef]
24. Li, Z.; Chan, K.W.; Hu, J. An Adaptive Fault Ride-Through Scheme for Grid-Forming Inverters Under Asymmetrical Grid Faults. *IEEE Trans. Ind. Electron.* **2022**, *69*, 12912–12923. [CrossRef]
25. Li, Z.; Hu, J.; Chan, K.W. A New Current Limiting and Overload Protection Scheme for Distributed Inverters in Microgrids Under Grid Faults. *IEEE Trans. Ind. Appl.* **2021**, *57*, 6362–6374. [CrossRef]
26. Chen, T.Y.; Chen, L.J.; Zheng, T.W. LVRT control method of virtual synchronous generator based on mode smooth switching. *Power Syst. Technol.* **2016**, *40*, 2134–2140.
27. Shuai, Z.K.; Shen, C.; Liu, X.; Li, Z. Transient angle stability of virtual synchronous generators using lyapunov's direct method. *IEEE Trans. Smart Grid.* **2019**, *10*, 4648–4661. [CrossRef]
28. Wu, H.; Wang, X.F. A mode-adaptive power-angle control method for transient stability enhancement of virtual synchronous generators. *IEEE J. Emerg. Sel. Topics Power Electron.* **2020**, *8*, 1034–1049. [CrossRef]
29. Pan, D.H.; Wang, X.-F.; Liu, F.-C. Transient stability of voltage-source converters with grid-forming control: A design-oriented study. *IEEE J. Emerg. Sel. Topics Power Electron.* **2020**, *8*, 1019–1033. [CrossRef]
30. Sun, K.; Yao, W.; Wen, J.Y.; Jiang, L. A two-stage simultaneous control scheme for the transient angle stability of VSG considering current limitation and voltage support. *IEEE Trans. Power Syst.* **2022**, *37*, 2137–2150. [CrossRef]
31. Chen, M.; Zhou, D.; Frede, B. Enhanced transient angle stability control of Grid-Forming converter based on virtual synchronous generator. *IEEE Trans. Ind. Electron.* **2022**, *69*, 9133–9144. [CrossRef]
32. *VDE-AR-N 4120*; Technical Requirements for the Connection and Operation of Customer Installations to the High-Voltage Network. VDE: Frankfurt, Germany, 2018.
33. *GB/T 37408-2019*; State Administration for Market Regulation, Standardization Administration of the People's Republic of China. Technical Requirements for Photovoltaic Gird-Connected Inverter. Standards Press of China: Beijing, China, 2019. (In Chinese)
34. Xiong, X.; Wu, C.; Hu, B.; Pan, D.; Blaabjerg, F. Transient Damping Method for Improving the Synchronization Stability of Virtual Synchronous Generators. *IEEE Trans. Power Electron.* **2021**, *36*, 7820–7831. [CrossRef]
35. Taul, M.G.; Golestan, S.; Wang, X.; Davari, P.; Blaabjerg, F. Modeling of Converter Synchronization Stability Under Grid Faults: The General Case. *IEEE J. Emerg. Sel. Topics Power Electron.* **2022**, *10*, 2790–2804. [CrossRef]